
Article:
Xiao, J., Tomczyk, M., Reaney, I.M. orcid.org/0000-0003-3893-6544 et al. (1 more author) (2018) Tailoring ferroelectric properties of 0.37BiScO3-0.63PbTiO3 thin films using a multifunctional LaNiO3 interlayer. Crystal Growth and Design, 18 (7). pp. 4037-4044. ISSN 1528-7483

https://doi.org/10.1021/acs.cgd.8b00412

(revised version paper ID cg-2018-00412q submitted to Crystal Growth & Design, May 2018)

Tailoring ferroelectric properties of 0.37$BiScO_3$-0.63$PbTiO_3$ thin films using a multifunctional $LaNiO_3$ interlayer

Jingzhong XIAO[‡†], Monika TOMCZYK[‡], Ian M. REANEY[§], Paula M. VILARINHO[‡*]

[†]CEMDRX, Department of Physics, University of Coimbra, Rua Larga, 3004-516 Coimbra, Portugal

[‡]Department of Materials and Ceramic Engineering, Centre for Research in Ceramics and Composite Materials, CICECO, University of Aveiro, 3810-193 Aveiro, Portugal

[§]Department of Materials Science and Engineering, University of Sheffield, Sir Robert Hadfield Building, Mappin Street, Sheffield, S1 3JD, UK[‡]

*Corresponding author: paula.vilarinho@ua.pt

ABSTRACT: Functional oxide thin films integrated into CMOS technology often exhibit degraded properties with respect to bulk materials because of complex interfacial phenomena. In this contribution, we demonstrate that a sol-gel $LaNiO_3$ (LNO) interlayer deposited onto the surface of a $Pt/TiO_2/SiO_2/Si$ substrate prior to growth of sol-gel $BiScO_3$-$PbTiO_3$ (BSPT) films acts: i) to seed nucleation of perovskite structured; ii) to template growth to give controlled orientation and enhanced crystallinity and iii) as a sink for oxygen vacancies (V_O). The LNO interlayer therefore not only improves the ferroelectric, piezoelectric and dielectric properties but also reduces leakage current and prevents degradation of the remanent polarization during fatigue tests. We propose that the use of a LNO interfacial layer may offer a generic solution to interfacial degradation in functional oxide films.

KEYWORDS: Functional oxide thin films, interfacial degradation, chemical

solution deposition, ferroelectricity

INTRODUCTION

Ferroelectric thin films have been extensively developed for applications such as microactuators, microsensors, ultrasonic motors, and micropumps.[1] Many such devices require direct integration of a ferroelectric film into Complementary Metal Oxide Semiconductor (CMOS) technology, typically using $Pt/TiO_2/SiO_2/Si$ substrates.[2] However, ferroelectric thin films such as $Pb(Zr_xTi_{1-x})O_3$ (PZT) deposited on Pt substrates generally possess poorer dielectric, ferroelectric and piezoelectric properties in comparison with ceramics and single crystals,[4,5] partially limiting their widespread usage. This degradation in performance is commonly attributed to interfacial effects that induce internal stress, modify the local defect chemistry and create non-optimised crystallographic orientations.[6] In principle, these limitations may be minimized if a suitable functional interlayer is introduced between the film and the Pt electrode.

So-called '*seed layers'* are known to control perovskite nucleation, reduce the temperature of phase formation, improve the film crystalline degree, suppress the formation of planar defects, and prevent reaction between films and substrates. [6-10] Seed layers have been extensively used on $Pt/Ti/SiO_2/Si$ bottom electrodes to overcome the detrimental effects of microstructural heterogeneities and variations in the crystalline quality of the films and are known to prevent deterioration of the ferroelectric properties. [11] So-called '*buffer layers'* between the ferroelectric film and platinized silicon substrate modify the residual stress state [12,13] which has a significant effect on the ferroelectric, piezoelectric and dielectric properties and, along with 'seed-layers', have been used to control film orientation.[14,15] In addition, to the use of buffer and seed layers, it has been known for many years that oxide electrodes used instead of plantinum (Pt on $Ti/SiO_2/Si$) improve performance since they prevent undesired compositional modification and impede charge interdiffusion processes.[16-19] **Table I** describes some examples of the effect of interlayers on ferroelectric films.

The above approaches for film optimization are generally used separately but if seeding, buffering and templating can be combined within a single multifunctiomal conducting oxide interlayer, there is great potential for optimization of film performance. In this contribution, we explore the use of a $LaNiO_3$ (LNO) multifunctional interlayer as a means to improve the dielectric, ferroelectric, piezoelectric and fatigue properties of $BiScO_3$-$PbTiO_3$ films.

Morphotropic phase boundary (MPB) $Pb(Zr,Ti)O_3$ (PZT) is the material of choice for many piezoelectric applications but the comparatively low Curie temperature (Tc) (380 ^oC), limits its utilization to ~250 ^oC [20] above which it tends to depole under high fields. More recently, MPB $BiScO_3$-$PbTiO_3$ (BSPT) has been proposed for high temperature piezoelectric applications due its higher T_C (450 ^oC) and excellent properties, superior even to PZT. [20-23] Further research is however, required to optimise thin film BSPT for integration into CMOS.[24] Trolier-McKinstry et al successfully fabricated rhombohedral (50/50) and (40/60) BSPT thin films on $SrRuO_3$/(100) $LaAlO_3$ substrates by pulsed laser deposition [25,26]. Xiaohui Wang et al deposited BSPT thin films on platinized silicon substrates ($Pt/TiO_2/SiO_2/Si$) by sol-gel method. These authors reported a dielectric constant and loss of 1200, and 0.05, respectively, remanent polarization of 33 μCcm^{-2} and coercive field of 220 kV/cm.[27-29] Morphotropic phase boundary BSPT thin films were also fabricated using $La_{0.7}Sr_{0.3}MnO_3$ (LSMO) as bottom electrodes on silicon substrates via a sol–gel method. The remanent polarization and coercive field of BSPT/LSMO were 28 μCcm^{-2} and 200 $kVcm^{-1}$, respectively. The films had a room-temperature dielectric constant of 720. The room-temperature piezoelectric coefficient d_{33} of 35 pm/V was observed.[30] $PbTiO_3$ seed-layers on $Pt/TiO_2/SiO_2/Si$ and $IrO_2/TiO_2/SiO_2/Si$ electrodes have been used to optimize the fabrication of sol-gel MPB $0.37BiScO_3$-$0.63PbTiO_3$ thin films [31,32] with improved electrical properties (ε_r = 1600, tanδ = 0.02, Pr ~ 23-30 $\mu C\ cm^{-2}$, E_C ~ 30-60 $kVcm^{-1}$).

Perovskite-structured $LaNiO_3$ (LNO) is a conductive oxide, which shows potential as an ideal multifunctional interlayer. [33-35] It can act as a source of oxygen during heat treatment that prevents the interdiffusion of vacancies between the

ferroelectric film and substrate and may also reduce the activation energy for nucleation of BSPT due its lattice match with MPB BSPT (LNO, a ~ 0.384 nm, BSPT, a = 0.405) [36]. Previously, sol-gel derived LNO had been adopted as an interlayer between the film and electrode to achieve highly textured PZT and (Pb, La)TiO_3 (PLT) thin films, [37-43] and enhance their electrical properties. As an oxide electrode or seeding layer, LNO also plays an important role in fabricating lead-free ferroelectric thin films, which are desirable alternative materials to the lead based ferroelectrics for the sake of environmental protection that needs the elimination of lead usage.[44-45] Here, sol-gel deposited LNO is proposed as a multifunctional interlayer to enhance the properties of sol-gel BSPT films deposited on $Pt/TiO_2/SiO_2/Si$ substrates. The effect of LNO layers on the structural and electrical performance of sol-gel derived BSPT thin films is systematically addressed and the potential for the wider use of LNO in optimizing functional thin films discussed.

EXPERIMENTAL SECTION

2.1 Materials. Lanthanum nitrate hexahydrate [$La(NO_3)_3 \cdot 6H_2O$] (Merck, 99%) , nickel (II) nitrate hexahydrate [$Ni(NO_3)_2 \cdot 6H_2O$] (Fluka, 98.5%), ethanol absolute (Merck, 99.8%) and formamide (Merck, 99.5%), lead acetate ($Pb(COOCH_3)_2$) (Panreac Company, 99.5%), bismuth nitrate ($Bi(NO_3)_3$) (Sigma-Aldrich, 99.99+%), scandium acetate ($Sc(COOCH_3)_3$ (Sigma-Aldrich, 99.9%), titanium isopropoxide ($Ti(i\text{-}Pr)_4$) (Sigma-Aldrich, >97%), glacial acetic acid (Pronalab, 100%), 2-propanol solutions (Fluka, 99.8%), acetylacetone (Merck, 99.5%), deionized water, $Pt/TiO_2/SiO_2/Si$ platinized silicon substrates.

2.2 Deposition of $LaNiO_3$ Films. Based on a wet chemical solution route, [37] the deposition of conductive LNO films on $Pt/TiO_2/SiO_2/Si$ was carried out. Lanthanum nitrate hexahydrate and nickel (II) nitrate hexahydrate were dissolved respectively in deionized water, and mixed in the stoichiometric ratio of La:Ni=1:1. To improve the solution wettability and avoid film cracking during heating, ethanol absolute and formamide were also added, until the resultant concentration of LNO solution was

diluted to 0.2 M. The LNO films were deposited by spinning the solution on $Pt/TiO_2/SiO_2/Si$ substrates at 4500 rpm for 40 s and annealed at 700 °C for 30 min for getting high quality layers.

2.3 Deposition of $BiScO_3$-$PbTiO_3$ (BSPT) Films. A 0.2M precursor solution with the composition ratio of $0.37BiScO_3$-$0.63PbTiO_3$ [BSPT (37/63)] was synthesizedby dissolving lead acetate, bismuth nitride, scandium acetate, and titanium isopropoxide into the solvents composed of glacial acetic acid, 2-propanol solutions, deionized water, and acetylacetone. [31,32] Formamide was added to improve the adhesion of the film to the substrate. BSPT films were deposited with a spin rate of 3000-5000 rpm and a spin time of 30 s. Each layer was dried at 350 ^oC and pyrolyzed at 650 ^oC for 5 min. After all the 10 layers had been deposited, the BSPT films on LNO electrodes (hereafter abbreviated as BSPT/LNO) with the desired thickness (~550 nm) were heat treated at 750 ^oC for 2 h for annealing. For comparison, BSPT thin films on $Pt/TiO_2/SiO_2/Si$ (150nm/20nm/300nm/Si substrate) (hereafter abbreviated as BSPT/Pt) were prepared under identical conditions as well. BSPT/LNO and BSPT/Pt film layer structures is schematically represented in **Figure 1**.

2.4 Structural and Morphology Characterization. The structure and phase evolution of the films were analyzed by x-ray θ-2θ diffraction (XRD, with a CuK α radiation, Rigaku, D/Max-B). X-ray rocking curves were obtained by tilting the BSPT films through the Bragg angle of the (200) plane. The X-ray pole figure measurements were performed with a Philips XPert MRD diffractometer using a Cu KR X-ray source. In the pole figure measurements the diffracted intensity was collected at a step-size of 5^o in the tilting and rotating angles in the whole hemisphere, at a fixed θ-2θ angle of the open detector that corresponds to the (200) reflections of BST films on Pt and LNO. The specimens were tilted and azimuthally rotated in relation to the incident beam. Surface and cross-sectional microstructure of the films were observed by scanning electron microscopy (SEM).

2.5 Dielectric and Ferroelectric Measurements. For electrical measurements,

gold top electrodes with a diameter of 0.6 mm were deposited on the films by dc sputtering using a shadow mask followed by an annealing treatment at 300 ºC for 30 min in air. The dielectric constant and loss of BSPT/LNO and BSPT/Pt capacitors as a function of frequency at room temperature were measured with an HP4284 Precision LCR Meter. The ferroelectric properties and fatigue behaviour were measured using a TF analyzer (TFA-1000) at room temperature. The current - electric field curves (I - V) were measured using a Keithley-617 electrometer at room temperature.

2.6 Local Piezoelectric Measurements. A modified commercial atomic force microscope (Multimode, Nanoscope IIIA, Digital Instruments) was used in the experiments for investigating the local piezoelectric response. A conductive Pt coated Si tip–cantilever (EFM-20, Resonance frequency: 75 kHz / Force constant: 2.8 N/m) system was used for the application of external voltages and for vibration detection. Ferroelectric thin films were excited by an external ac voltage V_{ac} applied between the PFM tip and the bottom electrode, and the deflection signal from the cantilever was detected by a lock-in amplifier. A topographic image of the film surface was taken simultaneously with the domain image. In the piezoelectric image, domains with opposite polarities exhibit different contrast. The local piezoelectric hysteresis loops (piezoloops) were measured inside individual grains. The loop acquisition consists of applying a dc voltage, V_{dc}, for a short time and measuring the effective piezoelectric response between the pulses. In this work, the absolute values of d_{33} were not determined, and all data are given for the relative piezo-response values measured in volts (output analogue signal of the lock-in amplifier). Since the results were obtained with the same cantilever and identical scanning and acquisition conditions, the comparison could be made for the relative values of local piezoelectric coefficients in BSPT films on Pt and LNO electrodes.

RESULTS AND DISCUSSION

MPB $BiScO_3$-$PbTiO_3$ (BSPT) thin films were deposited by chemical solution deposition under identical conditions on Pt/TiO_2/SiO_2/Si (150nm/20nm/300nm/Si

substrate) (BSPT/Pt) and on LNO/Pt/TiO_2/SiO_2/Si (BSPT/LNO). The LNO on the former substrate was deposited using a sol-gel technique.

Figure 2 illustrates the X-ray Diffraction (XRD) patterns of BSPT films grown on Pt and LNO layers, with an annealing treatment at 750 ^oC for 2 h. All film peaks are attributed to perovskite and no second phases were observed. BSPT/Pt films possessed no preferred crystallographic orientation but comparison with polycrystalline patterns suggested that BSPT/LNO have a preferred h00 texture. The Lotgering factor (f) may be used to calculate the degree of (100)-texture for BSPT/LNO films [38]

$$f = \frac{p - p_0}{1 - p_0}, \qquad (1)$$

$$p = \frac{\sum I(h00)}{\sum I(hkl)}, \qquad (2)$$

where $p = p_0$ is the orientation intensity ratio for randomly oriented samples. The f factors of BSPT/Pt and BSPT/LNO thin films were calculated as 0.62 and 0.94, respectively.

In the XRD patterns near 40^o, BSPT/Pt exhibits a wide band which indicates that the peak consist both Pt (111) and BSPT (111) diffractions, while BSPT/LNO only exhibits a narrow Pt (111) diffraction peak, which also means that no BSPT (111) diffraction was observed near this area.

To analyse further the preferred (h00) orientation of BSPT/LNO films, XRD rocking curves and pole figures were obtained. The rocking curve (**Figure 3**) revealed that BSPT/LNO films have an intense, narrow (200) peak in contrast to BSPT/Pt. **Figure 4** depicts the X-ray pole figure distribution of BSPT/LNO and BSPT/Pt, corresponding to (200) reflections. In the case of BSPT/LNO, only a strong diffraction point appears at the center of the (200) ring-type reflection peak, which indicates a strong film texture. For BSPT/Pt, distinct diffraction concentrations not only appear at the peak center, but also spread over other ring bands, indicating only,

at best, weak (h00) texture.

In addition to the texture described in detail above, the full width at half maximum (FWHM) of the (100) diffraction for BSPT/Pt and BSPT/LNO films were for 0.30^{o} and 0.24^{o}, respectively; a low FWHM value indicates a strong film texture. The introduction of the LNO layer therefore not only promotes (h00) texture but also increases the average coherently diffracting volume, which qualitatively equates to improved crystallinity.

Figure 5 shows Scanning Electron Microscopy (SEM) cross-section and top view images of BSPT/LNO and BSPT/Pt films. Some pinholes can be observed from the top view microstructures but the cross-sections indicate that both the BSPT/Pt and BSPT/LNO thin films are dense and ~550 nm thick. The BSPT/Pt interface appears sharp in these images but the BSPT/LNO interface is less well defined in **Figure 5**. It is proposed that the BSPT/LNO interface decreases the activation energy for nucleation due to local epitaxial growth of the film on the interlayer, thereby accounting for the absence of a well defined interface in the SEM observation.[38] In contrast, BSPT/Pt film is essentially polycrystalline with no distinct orientation relation with the electrode. The local epitaxial growth of BSPT on LNO also accounts for the effective increase in crystallinity, as determined from the reduction in FWHM (full with half maximum) of the X-ray diffraction peaks in **Figure 2**. The BSPT/LNO films are composed of columnar grains but the BSPT/Pt films have no discernible grain structure in the SEM images. In the surface SEM images, BSPT/LNO film exhibits both the large and small group grains that evidently exhibiting a regular shape, which indicates the film has a better crystalline degree than the BSPT/Pt one, although some small grains seem to be smaller than those in BSPT/Pt films. We expect that these two groups of grains could be ascribed to different growth dynamics for BSPT/LNO, that the large grain growth behaviour is possibly based on the columnar grain growth as shown in **Figure 5 (b)**, while the small grain growth behaviour is more random, which possibly provides valuable information for optimizing the film growth condition and parameters, and improving the film quality in the future. Due to the observed differences in microstructure and film orientation additional TEM

experiments were performed in order to study early crystallization stages of BSPT on distinct bottom electrodes. **Figure 5** shows the Transmission Electron Microscopy (TEM) cross-section images of BSPT/LNO and BSPT/Pt films annealed at 500 ^{o}C, from which one can observed that BSPT/Pt film presents amorphous matter, while BSPT/LNO is partly crystalline with a columnar growth morphology. TEM observation corroborates that LNO layer indeed improves BSPT film quality and promotes perovskite formation..

The dielectric and polarization-electric field measurements were performed to assess the influence of LNO interlayer on functional properties. **Figure 6** depicts the frequency dependence of the dielectric constant and dielectric loss of the BSPT thin films on Pt and LNO electrodes. The BSPT films on LNO electrodes exhibited higher dielectric permittivity (2250) and lower loss (0.02) than those on Pt electrodes and superior to those reported previously at 100 kHz. [26-29]

Figure 7 (a) shows the polarization (P-E) hysteresis loops for BSPT/LNO and BSPT/Pt measured at room temperature and at 100 Hz with the maximum applied voltage of 12 V. BSPT/LNO thin films exhibit a remanent polarization (P_r) of 40 $\mu C.cm^{-2}$ and a coercive field (E_c) of ~68 $kV.cm^{-1}$ in comparison with values of about 25 $\mu C.cm^{-2}$ and 60 $kV.cm^{-1}$, respectively for BSPT/Pt. Although the LNO interlayer slightly increases the coercive field (only increasing 13%), it substantially enhances the remanent polarization (increasing 60%) and promotes a saturated hysteresis loop as a result of enhanced orientation and crystallinity with respect to BSPT/Pt films. [4, 37-42]

Figure 7 (b) shows the fatigue behaviour of BSPT films on Pt and LNO electrodes up to 2×10^9 bipolar switching cycles. A clear improvement of the fatigue of BSPT/LNO films was observed with respect to BSPT/Pt. BSPT/Pt films begin to exhibit fatigue behaviour from 10^7 cycles, and after 2×10^9 cycles, significant degradation of the P_r was observed. In comparison, no decrease of remnant polarization was observed for BSPT/LNO films until 2×10^9 cycles. It is proposed that the presence of the LNO interlayer acts as a sink for $V_{O^{\cdot\cdot}}$ that accumulates at the interface during polarization reversal,[43] thereby eliminating space-charge layers that act to nullify remanent polarization. [46]

The leakage current density under different electrical fields for BSPT/LNO and BSPT/Pt thin films is shown in **Figure 8**. The leakage current curve of BSPT/LNO exhibits nonlinear behaviours, and LNO decreases the leakage current and current density, in consistency with low loss and saturated hysteresis curves; this also proves that LNO layer can act as a sink for oxygen vacancies, due to its high oxygen affinity avoiding the migration of space charges at the electrode–film interface.

Using piezo-force response microscopy (PFM), the local polarization behaviour and piezoelectric properties were further investigated. The top-left parts inside **Figure 9 (a) and (b)** show the AFM topographic images of BSPT/Pt and BSPT/LNO films, which indicate an average grain size lower than 100 nm. In the piezoresponse images shown in the bottom-right parts of **Figure 9 (a) and (b)**, domains with opposite polarization exhibit different contrast. Dark regions (negative domains) correspond to domains with polarization oriented towards the substrate, and the polarization in bright regions (positive domains) pointed to the surface of the film.[47] The central part of **Figure 9 (a) and (b)** depicts the local piezoelectric hysteresis loops (piezoloops) of BSPT/Pt and BSPT/LNO measured on a fixed point inside a bright domain (as shown in the cross points in the piezoresponse images). From these loops one can observe that under the applied voltage of 10 V, the maximum relative d_{33} of BSPT/LNO is higher than that of BSPT/Pt, in agreement with the enhanced crystallinity and (h00) texture; accordingly, d_{33} is known to be optimized in the (100) direction of tetragonal phase. [48]

However the effect that the LNO interlayer has on residual stress in BSPT films cannot be also ignored. [4,41] The total residual stress (S_t) consists of three parts: [49]

$$S_t = S_i + S_{th} + S_e , \qquad (3)$$

where S_i, S_{th}, S_e stands for the intrinsic stress, thermal stress, and extrinsic stress, respectively. The intrinsic stress is induced by the formation of the grain boundaries as the crystal grain grows and interacts with neighboring grains. Thermal stress is

induced by the mismatch between thermal expansion coefficients of the ferroelectric film and the substrate. The extrinsic stress originates from lattice parameter mismatch between film and the substrate [49] and for a relaxed, textured film such as considered here, may be ignored.

From the above considerations therefore, the LNO interlayer may tailor the residual stress in several ways. [33-35] First, the LNO layer induces columnar growth which decreases the intrinsic stress associated with grain boundaries. Second, the thermal expansion coefficient of BSPT (~10^{-5}/K) is similar to that of LNO (8.2×10^{-6}/K) but dissimilar to that of Pt (27×10^{-6}/K). The LNO can thus act as a buffer layer and decreases the thermal stress in the films of BSPT/LNO.

For further understanding and analysis of the effect of stress on the properties, lattice and thermal expansion coefficients of BSPT and substrates are listed in **Table II**. From the thermal expansion coefficient mismatch between ferroelectric materials and substrates, we may conclude that the stress in BSPT films on LNO is compressive stress, while in BSPT/Pt films is tensile stress. According to some reports on other ferroelectric systems,[50] compressive stresses between films and substrates favours c-domain switching and leads to large polarization and strong ferroelectric behaviours, while tensile stresses triggers the opposite effect, as characterized by measurements of dielectric constants and polarization hysteresis loops. In the results of this work (as shown in **Fig.5, Fig.7 and Fig.9**), the fact that BSPT/LNO exhibits better dielectric and ferroelectric properties than those of BSPT/Pt confirms the previous observation, which indicates that the introduction of LNO layers between the BSPT and Pt further control and tailor the stress level that can significantly improve the properties of ferroelectric films.

In summary, we propose that the LNO interlayer templates film growth and enhances crystallinity and orientation, acts as a sink for V_O, and forms a buffer layer for reducing residual stress due to thermal expansion mismatch. The net result is a significant enhancement in ferroelectric, dielectric, piezoelectric and fatigue properties with respect to BSPT/Pt films.

CONCLUSIONS

We have demonstrated using BSPT (37/63) films as proof of concept, that tailoring of the properties (fatigue, loss, ε_r, d_{33}, P_R) of ferroelectric thin film can be realized through the use of a multifunctional interlayer. In this case study, LNO thin films were successfully deposited on a $Pt/TiO_2/SiO_2/Si$ substrate by a sol-gel technique followed by the deposition of BSPT (37/63) MPB thin films. The interlayer simultaneously acted as: i) a seed layer to reduce the activation energy for crystallisation of the perovskite, ii) a template to induce a highly (h00) textured orientation accompanied by improved crystallinity, and iii) a sink for V_O that build up at the interface during polarization reversal (fatigue) experiments. The use of an interlayer improved P_r, ε_r and fatigue behaviour and decreased dielectric loss and leakage current density. We propose that multifunctional interlayers of this type could provide a valuable generic strategy for tailoring the properties of functional ceramic films.

AUTHORS INFORMATION

Corresponding Author

*E-mail: paula.vilarinho@ua.pt (Prof. Paula M. Vilarinho, website of her group: www.electroceramicsgroup.org)

ORCID: https://orcid.org/0000-0001-5161-1360

The authors declare no competing financial issues

ACKNOWLEDGEMENTS

This work was funded by FEDER funds via Programa Operacional Factores de Competitividade – COMPETE and National funds via FCT (Fundação para a Ciência e Tecnologia) within the Project CICECO - FCOMP-01-0124-FEDER-037271 (FCT PEst-C/CTM/LA0011/2013). I. M. Reaney acknowledges the support of the

Engineering and Physical Sciences Research Council grant, EP/L017563/1.

DEDICATION

This paper is dedicated to the memory of Aiying Wu.

REFERENCES

(1) Setter N.; Damjanovic D.; L Eng.; Fox G.; Gevorgian S.; Hong S.; Kingon A.; Kohlstedt H.; Park N. Y.; Ferroelectric thin films: Review of materials, properties, and applications, Journal of Applied Physics. **2006**, 100, 5, 051606.

(2) Shelton, C. T.; Kotula, P. G.; Brennecka, G. L.; Lam, P. G.; Meyer, K. E.; Maria, J.; Gibbons, B. J.; Ihlefeld, J. F.; Chemically homogeneous complex oxide thin films via improved substrate metallization, Adv. Func.Mater. **2012**, 22, 2295.

(3) Wang, Y.; Ganpule, C.; Liu, B.; Li, H.; Mori, K.; Hill, B.; Wuttig, M.; Ramesh, R.; Epitaxial ferroelectric $Pb(Zr,Ti)O_3$ thin films on Si using $SrTiO_3$ template layers, Appl. Phys. Lett. **2002**, 80, 97.

(4) Kim, D.; Maria, J.; Kingon, K.; Streiffer, S.; Evaluation of intrinsic and extrinsic contributions to the piezoelectric properties of $Pb(Zr_{1-X}Ti_X)O_3$ thin films as a function of composition, J. Appl. Phys. **2003**, 93, 5568.

(5) Pérez de la Cruz J.; Joanni E.; Vilarinho P. M.; Kholkin A. L.; Thickness effect on the dielectric, ferroelectric, and piezoelectric properties of ferroelectric lead zirconate titanate thin films, J. Appl. Phys. **2010**, 108, 114106-1.

(6) Wu, A.; Vilarinho, P. M.; Reaney, I. Salvado, M.; Early stages of crystallization of sol−gel-derived lead zirconate titanate thin films, Chem. Mater. **2003**, 15, 1147.

(7) Kwok, C.; Desu, S.; Low temperature perovskite formation of lead zirconate titanate thin films by a seeding process**,** J. Mater. Res. **1993**, 8, 339.

(8) Suzuki, H.; Koizumi, T.; Kondo, Y.; Kaneko, S.; Low-temperature processing of $Pb(Zr_{0\cdot53}Ti_{0\cdot47})O_3$ thin film from stable precursor sol, J. Eur. Ceram. Soc. **1999**, 19, 1397.

(9) Zeng, J.; Zhang, M.; Wang. L.; Lin, C.; Influence of lead titanate seed layer on orientation behaviour and ferroelectric characteristics of sol-gel derived PZT thin films, J. Phys.: Condens. Matter. **1999**, 11, 1139.

(10) Fu, Z.; Wu, A.; Vilarinho, P. M.; Effect of seed layer thickness on texture and electrical properties of sol−gel derived $(Ba_{0.8}Sr_{0.2})TiO_3$ thin films, Chem. Mater. **2006**, 18, 3343.

(11) Muralt P.; Ferroelectric thin films for micro-sensors and actuators: a review, J. Micromech. Microeng. **2000**, 10**,** 136.

(12) Taylor, D.; Damjanovic, D.; Piezoelectric properties of rhombohedral $Pb(Zr,Ti)O_3$ thin films with (100), (111), and "random" crystallographic orientation, Appl. Phys. Lett. **2000**, 76, 1615.

(13) Liu, S.; Ma, B.; Narayanan, M.; Chao, S.; Koritala, S.; Balachandran, U.; Improved properties of barium strontium titanate thin films grown on copper foils by pulsed laser deposition using a self-buffered layer, J. Phys. D: Appl. Phys. **2012**, 45, 175304.

(14) Ramesh, R.; Schlom, D.; Orienting Ferroelectric Films, Science. **2002**, 296, 1975.

(15) Ranjith, R.; Chaudhuri, A.; Krupanidhi, S.; Victor, P.; Role of template layer on microstructure, phase formation and polarization behavior of ferroelectric relaxor thin films, J. Appl. Phys. **2007**, 101, 104111.

(16) Yang, Y.; Lee, S.; Kim, S.; Chae, B.; Jang, M.; Schottky barrier effects in the electronic conduction of sol–gel derived lead zirconate titanate thin film capacitors, J. Appl. Phys. **1998**, 84,5005.

(17) Nakamura, T.; Nakao, Y.; Kamisawa, A.; Takasu, H.; Preparation of Pb(Zr,Ti)O_3 thin films on electrodes including IrO_2, Appl. Phys. Lett. **1994**, 65, 1522.

(18) Genechten, D.; Vanhoyland, G.; Haen, J.; Johnson, J.; Wouters, D.; Phase evolution of sol–gel prepared $Pb(Zr_{0.3}Ti_{0.7})O_3$ thin films deposited on $IrO_2/TiO_2/SiO_2$/Si electrodes, Thin Solid Films **2004**, 467, 104.

(19) Wang, Z.; Chu, J.; Maeda, R.; Kokawa, H.; Effect of bottom electrodes on microstructures and electrical properties of sol–gel derived $Pb(Zr_{0.53}Ti_{0.47})O_3$ thin films, Thin Solid Films **2002**, 416, 66.

(20) Eitel, R. E.; Randall, C. A.; Shrout, T. R.; Rehrig, P. R.; Wackenberger, W.; Park, S. -E.; New high temperature morphotropic phase boundary piezoelectrics based on Bi(Me)O_3–$PbTiO_3$ ceramics, Jap. J. Appl. Phys. **2001**, 40, 5999.

(21) Eitel, R. E.; Zhang, S.; Shrout, T. R.; Randall, C. A.; Phase diagram of the perovskite system (1−x)$BiScO_3$-x$PbTiO_3$, J. Appl. Phys. **2004**, 96, 2828.

(22) Zhang, S.; Lebrun, L.; Rhee, S.; Eitel, R. E.; Randall, C. A.; Shrout, T. R.; Crystal growth and characterization of new high Curie temperature (1−x)$BiScO_3$–x$PbTiO_3$ single crystals, J. Cryst. Grow. **2002**, 236, 210.

(23) Zou, T.; Wang, X.; Wang, X.; Zhong, C.; Li, L.; Chen, I. -W.; Bulk dense fine-grain (1−x)$BiScO_3$–x$PbTiO_3$ ceramics with high piezoelectric coefficient, Appl. Phys. Lett. **2008**, 93, 192913.

(24) Liu, J. -M.; Pan, B.; Chan, H. L.; Zhu, S. N.; Zhu, Y. Y.; Liu, Z. G.; Piezoelectric coefficient measurement of piezoelectric thin films: an overview, Mater. Chem. Phys. **2002**, 75, 12.

(25) Yoshimura, T.; Trolier-McKinstry, S. Growth and properties of (001) $BiScO_3$–$PbTiO_3$ epitaxial films, Appl. Phys. Lett. **2002**, 81, 2065.

(26) Nino, J.; Trolier-McKinstry, S.; Dielectric, ferroelectric, and piezoelectric properties of (001) $BiScO_3$–$PbTiO_3$ epitaxial films near the morphotropic phase boundary, J. Mater. Res. **2004**, 19, 568.

(27) Wen, H.; Wang, X.; Deng, X.; Li, L.; Characterization of (100)-oriented $BiScO_3$–$PbTiO_3$ thin films synthesized by a modified sol-gel method, Appl. Phys. Lett. **2006**, 88, 222904.

(28) Wen, H.; Wang, X.; Zhong, C.; Shu, L. Li, L.; Epitaxial growth of sol-gel derived $BiScO_3$–$PbTiO_3$ thin film on Nb-doped $SrTiO_3$ single crystal substrate, Appl. Phys. Lett. **2007**, 90**,** 202902.

(29) Zhong, C.; Wang, X.; Li, L.; Fabrication and characterization of high curie temperature $BiSc_{1/2}Fe_{1/2}O_3$–$PbTiO_3$ piezoelectric films by a sol–gel process, Ceramics International, **2012**, 38S, S237.

(30) Zhang S., Dong X., Chen Y., Cao F., Zhang Y., Wang G., Sama N., Ramiens D.; Growth and electric properties of MPB $BiScO_3$–$PbTiO_3$ thin films on $La_{0.7}Sr_{0.3}MnO_3$-coated silicon substrates, J. Am. Ceram. Soc., **2010**, 93, 1583.

(31) Xiao, J.; Wu, A.; Vilarinho, P. M.; Sol-gel derived morphotropic phase boundary $0.37BiScO_3$–$0.63PbTiO_3$ thin films, Appl. Phys. Lett. **2008**, 92, 032902.

(32) Xiao, J.; Wu, A.; Vilarinho, P. M.; Ramos, R; Alves, E.; Electrical properties of sol–gel derived MPB $0.37BiScO_3$–$0.63PbTiO_3$ thin films deposited on iridium oxide electrodes, Journal of Materials Chemistry, **2009**, 19, 5572.

(33) Chen, M.; Wu, T.; Wu, J.; Effect of textured $LaNiO_3$ electrode on the fatigue improvement of $Pb(Zr_{0.53}Ti_{0.47})O_3$ thin films, Appl. Phys. Lett. **1996**, 68, 1430.

(34) Kang, B.; Kim, D.; Noh, E. T.; Polarization retention in $Pb(Zr_{0.4}Ti_{0.6})O_3$ capacitors with IrO_2 top electrodes, Appl. Phys. Lett. **2004**, 84, 3127.

(35) Nakamura, T.; Nakao, Y.; Kamisawa, A.; Takasu, H.; Electrical properties of PZT thin films with Ir and IrO_2, electrodes, IEEE, Proc. 9th Int.Symp. Application of Ferroelectrics, **1995**, 9, 547.

(36) Choa, C.; Francisa, L.; Pollab, D.; Ferroelectric properties of sol–gel deposited $Pb(Zr,Ti)O_3/LaNiO_3$ thin films on single crystal and platinized-Si substrates, Mater. Lett. **1999**, 38, 125.

(37) Bao, D.; Wakiya, N.; Shinozaki, K.; Mizutani, N.; Yao, X.; Improved electrical properties of $(Pb,La)TiO_3$ thin films using compositionally and structurally compatible $LaNiO_3$ thin films as bottom electrodes, Appl. Phys. Lett. **2001**, 78, 3286.

(38) Lotgering, F.; Topotactical reactions with ferrimagnetic oxides having hexagonal crystal structures—I, J. Inorg. Nucl. Chem. 1959, 9, 113.

(39) Li, Y.; Hu, Z.; Sun, J.; Meng, J.; Chu, J.; Effects of $LaNiO_3$ bottom electrode on structural and dielectric properties of $CaCu_3Ti_4O_{12}$ films fabricated by sol-gel method, Appl. Phys. Lett. **2008**, 92, 042901.

(40) Ahluwalia, R.; Lookman, T.; Saxena, A.; Domain-size dependence of piezoelectric properties of ferroelectrics, Phys. Rev. B **2005**, 72, 014112.

(41) Ramesh, R.; Inam, A.; Wilkens, A.; Chan, W. K. Sands, T.; Tarascon J. M.; Ferroelectric bismuth titanate/superconductor (Y-Ba-Cu-O) thin-film heterostructures on silicon, Appl. Phys. Lett. **1991**, 59, 1782.

(42) Lin, A.; Hong, X.; Wood, V.; Verevkin, A.; Ahn, C.; Epitaxial growth of $Pb(Zr_{0.2}Ti_{0.8})O_3$ on Si and its nanoscale piezoelectric properties, Appl. Phys. Lett. **2001**, 78, 2034.

(43) Chen, M.; Wu, T.; Wu, J.; Effect of textured $LaNiO_3$ electrode on the fatigue improvement of $Pb(Zr_{0.53}Ti_{0.47})O_3$ thin films, Appl. Phys. Lett. **1996**, 68, 1430.

(44) Zheng, X. J.; Dai, S. H.; Feng, X.; Zhang, Tong; Zhang D. Z.; Gong, Y. Q., Chen Y. Q.; He, L.; Structural and electrical properties of $(Na_{0.85}K_{0.15})_{0.5}Bi_{0.5}TiO_3$ thin films deposited on $LaNiO_3$ and Pt bottom electrodes, Appl. Surf. Sci., **2010**, 256, 3316.

(45) Lee Y. H., Wu J.M., Chueh Y. L., Chou L.J.; Low-temperature growth and interface characterization of $BiFeO_3$ thin films with reduced leakage current, Appl. Phys. Lett. **2005**, 87, 172901.

(46) Tagantsev, A. K.; Stolichnov, I.; Colla, E. L.; Setter, N.; Polarization fatigue in ferroelectric films: Basic experimental findings, phenomenological scenarios, and microscopic features, J. Appl. Phys. **2001**, 90, 1387.

(47) Gruverman, A.; Auciello, O.; Tokumoto, H.; Imaging and control of domain structures in ferroelectric thin films via scanning force microscopy, Annu. Rev. Mater. Sci. **1998**, 28, 101.

(48) Du, X.; Zheng, J.; Belegundu, U.; Uchino, U.; Crystal orientation dependence of piezoelectric properties of lead zirconate titanate near the morphotropic phase boundary, Appl. Phys. Lett. **1998**, 72, 2421.

(49) Lian, L.; Sottos, N.R.; Effects of thickness on the piezoelectric and dielectric properties of lead zirconate titanate thin films, J. Appl. Phys. **2000**, 87, 3941.

(50) Han, G.; Ryu, J.; Yoon, W.; Choi, J.; Hahn, B.; Kim, J.; Park, D.; Ahn, C.; Priya, S.; Jeong, D.; Stress-controlled $Pb(Zr_{0.52}Ti_{0.48})O_3$ thick films by thermal expansion mismatch between substrate and $Pb(Zr_{0.52}Ti_{0.48})O_3$ film, J. Appl. Phys. **2011**, 110, 124101.

Figure and table Captions:

Figure 1. Schematic representation of BSPT/LNO (a) and BSPT/Pt (b) film layer structures.

Figure 2. XRD curves of BSPT films grown on Pt and LNO layers, annealed at 750 ^{o}C for 2 hours. Both these films exhibit pure-phase perovskite structure and good crystalline degree; in comparison with the random BSPT film on Pt, a highly (h00) preferred crystallographic orientation is observed in BSPT / LNO films.

Figure 3. Rocking curves of BSPT thin films on Pt and LNO electrodes at (200) reflection. A dramatically intense and narrow (200) diffraction peak is observed in BSPT/LNO films (the FWHM of (200) of BSPT/LNO and BSPT/Pt is 2.2^{o} and 7.1^{o}), also demonstrating its high film texture degree, in contrast to the random BSPT/Pt films.

Figure 4. X-ray Pole figures of BSPT thin films. (a) corresponding to (200) reflection (2θ=45.23^{o}) of BSPT/LNO; (b) corresponding to (200) reflection (2θ=45.26^{o}) of BSPT/Pt. A (200) ring-type pole figure is observed for highly oriented BSPT / LNO film, while in the figure for BSPT / Pt film, the diffraction ring bands indicating a weak film orientation.

Figure 5. Cross section ((a) and (b)) and top view ((c) and (d)) SEM micrographs of BSPT 37/63 films on Pt/Ti/SiO_2/Si and LNO/Pt/Ti/SiO_2/Si. From the microstructure images, the fairly dense films are observed for both these two systems with the film thickness of about 550 nm. TEM Cross section micrographs of BSPT 37/63 films on Pt/Ti/SiO_2/Si and LNO/Pt/Ti/SiO_2/Si, annealed at 500 ^{o}C, (e) and (f). BSPT/Pt film exhibits amorphous, while BSPT/LNO shows partly crystalline mater and columnar growth morphology. The TEM observation also indicates LNO layer improve the film

quality in the early crystallization stage of BSPT films, which is consistent with SEM observations.

Figure 6. Frequency dependence of dielectric constant and dielectric losses of MPB BSPT (37/63) thin films on Pt and LNO electrodes. It is observed that the BSPT films on LNO electrodes exhibit higher dielectric permittivity and lower dielectric losses than those on Pt electrodes; particularly the use of LNO inter-layer increases about 67% for the permittivity value.

Figure 7. Polarization versus electric field of BSPT/LNO and BSPT/Pt films at 100 Hz and at room temperature (a); Fatigue behaviour of BSPT/LNO and BSPT/Pt till 2×10^9 switching cycles (b). The saturated polarization (P-E) hysteresis loops are observed for both the two samples, and BSPT/LNO films exhibit an evidently increase of 60% for remanent polarization value in comparison with BSPT / Pt films.
For the fatigue observation, BSPT/Pt films begin to exhibit fatigue feature from 10^7 cycles, while no decrease of remnant polarization and no fatigue behaviour was observed for the BSPT/LNO films until 2×10^9 cycles.

Figure 8. The leakage current density under different electrical fields of BSPT/LNO and BSPT/Pt thin films. Under the electrical field of 60 kV / cm, it is observed that the current density value of BSPT / LNO reduces about 40% in comparison with that of BSPT / Pt.

Figure 9. The top-left parts inside (a) and (b) indicate topography images of BSPT/Pt and BSPT/LNO obtained by Piezo Force Microscopy (PFM), with a roughness of BSPT / LNO (2.8 nm) and BSPT /Pt (3.4 nm). The piezoresponse images for BSPT / LNO and BSPT / Pt in the bottom-right parts of **Figure 9** (a) and (b) exhibit domains with opposite polarization exhibiting different contrast of dark regions (negative domains) and bright regions (positive domains) are observed. The central parts of **Figure 9** (a) and (b) exhibit local piezoelectric hysteresis loops (piezoloops) of

BSPT/Pt and BSPT/LNO measured by PFM under the applied voltage of 10 V. BSPT / LNO films exhibit a saturated local d_{33} loop, and the maximum relative d_{33} value is much higher than that of BSPT/Pt.

Table I Simple examples indication for the effect of interlayer on the ferroelectric films. The use of seed layers, oxide electrode layers, buffer layers and oriented epitaxial template layers have been separately used for the growth of ferroelectric films.

Table II Lattice and thermal expansion coefficient of the BSPT films, Pt, and LNO, as well as the remanent polarization of BSPT films on Pt and LNO.

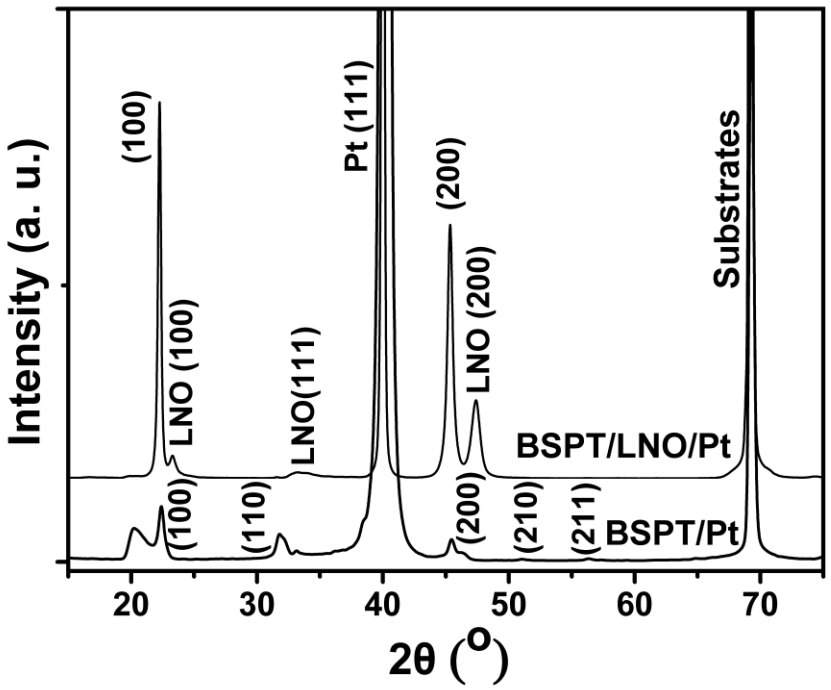
Intensity (a. u.)
(100)
LNO (100)
LNO(111)
Pt (111)
(200)
LNO (200)
Substrates
BSPT/LNO/Pt
(100)
(110)
(200)
(210)
(211)
BSPT/Pt
20
30
40
50
60
70
2θ (°)

Figure 2

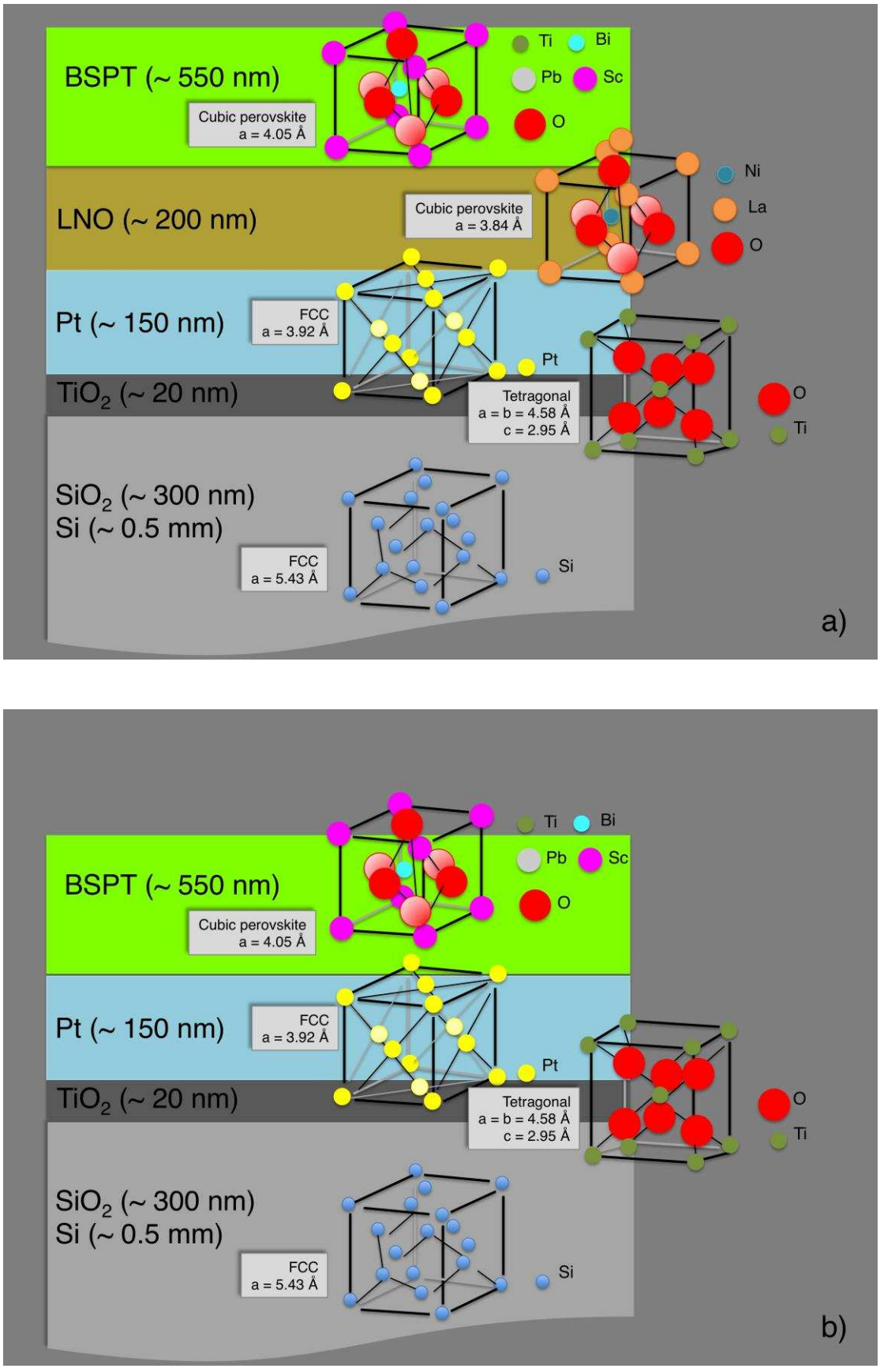
BSPT (~ 550 nm)
Cubic perovskite
a = 4.05 Å
Ti
Bi
Pb
Sc
O
LNO (~ 200 nm)
Cubic perovskite
a = 3.84 Å
Ni
La
O
Pt (~ 150 nm)
FCC
a = 3.92 Å
Pt
TiO2 (~ 20 nm)
Tetragonal
a = b = 4.58 Å
c = 2.95 Å
O
Ti
SiO2 (~ 300 nm)
Si (~ 0.5 mm)
FCC
a = 5.43 Å
Si
a)
BSPT (~ 550 nm)
Cubic perovskite
a = 4.05 Å
Ti
Bi
Pb
Sc
O
Pt (~ 150 nm)
FCC
a = 3.92 Å
Pt
TiO2 (~ 20 nm)
Tetragonal
a = b = 4.58 Å
c = 2.95 Å
O
Ti
SiO2 (~ 300 nm)
Si (~ 0.5 mm)
FCC
a = 5.43 Å
Si
b)

Figure 1

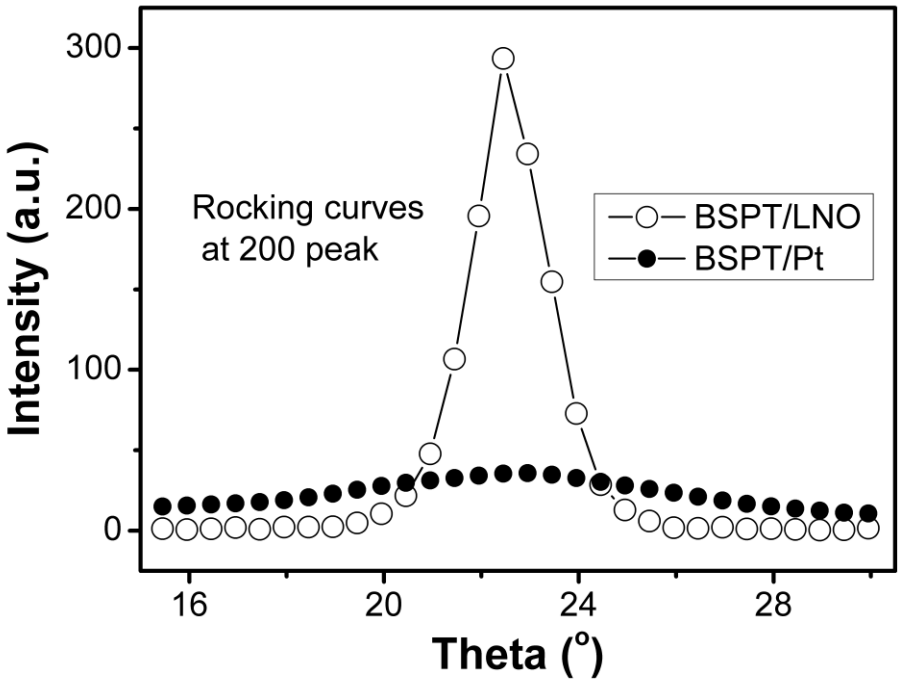
Intensity (a.u.)
300
200
100
0
Rocking curves
at 200 peak
BSPT/LNO
BSPT/Pt
16
20
24
28
Theta (°)

Figure 3

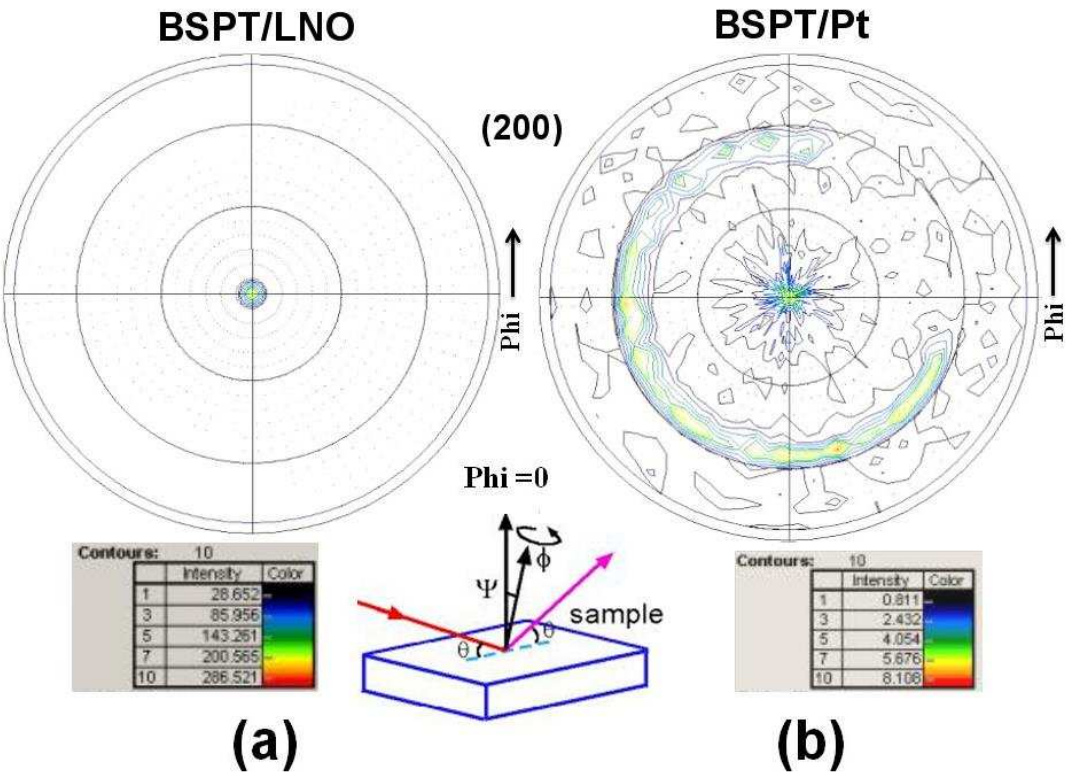
BSPT/LNO
BSPT/Pt
(200)
Phi
Phi
Phi =0
Contours: 10
Intensity Color
1 28.652
3 85.956
5 143.261
7 200.565
10 286.521
Contours: 10
Intensity Color
1 0.811
3 2.432
5 4.054
7 5.676
10 8.106
Ψ
ϕ
θ
θ
sample
(a)
(b)

Figure 4

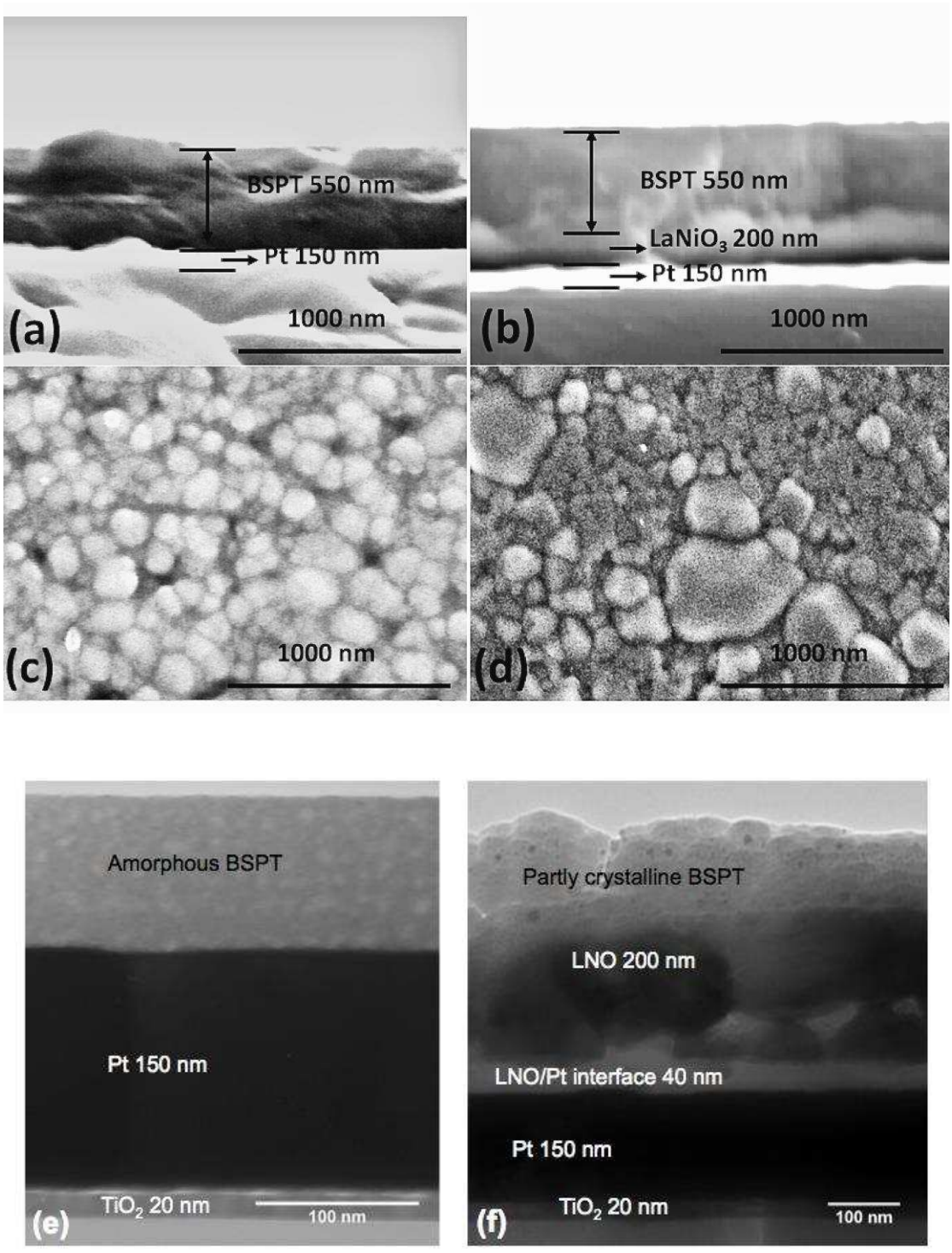
BSPT 550 nm
Pt 150 nm
1000 nm
(a)
BSPT 550 nm
LaNiO3 200 nm
Pt 150 nm
1000 nm
(b)
1000 nm
(c)
1000 nm
(d)
Amorphous BSPT
Pt 150 nm
TiO2 20 nm
100 nm
(e)
Partly crystalline BSPT
LNO 200 nm
LNO/Pt interface 40 nm
Pt 150 nm
TiO2 20 nm
100 nm
(f)

Figure 5

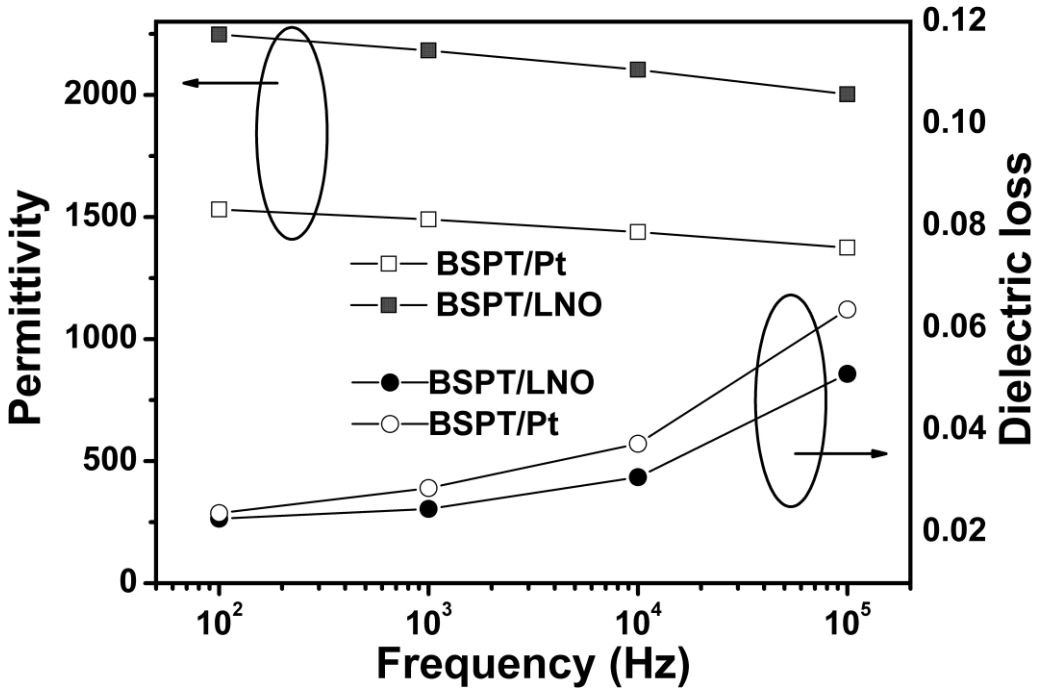
Permittivity
Dielectric loss
Frequency (Hz)
BSPT/Pt
BSPT/LNO
BSPT/LNO
BSPT/Pt
0
500
1000
1500
2000
0.02
0.04
0.06
0.08
0.10
0.12
10^2
10^3
10^4
10^5

Figure 6

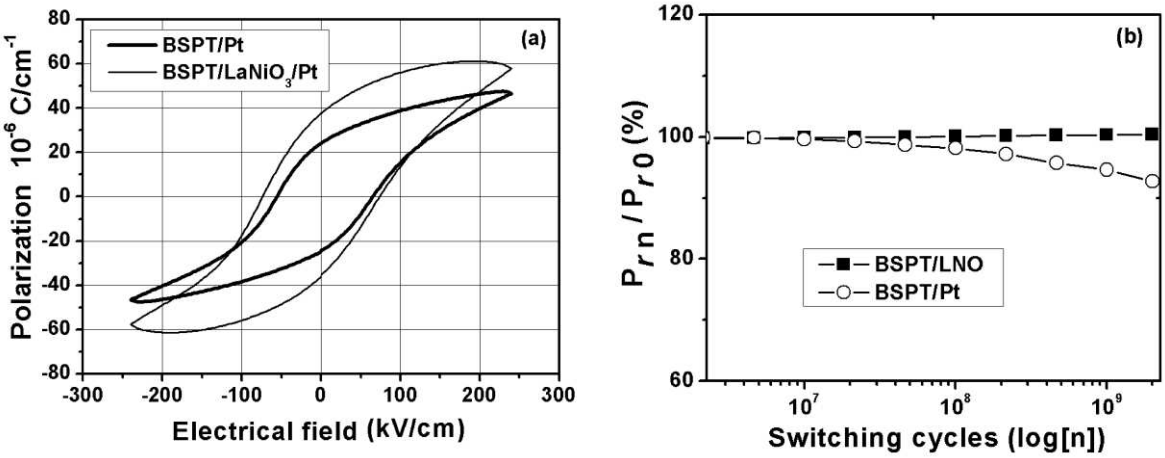
(a)
BSPT/Pt
BSPT/LaNiO3/Pt
Polarization 10-6 C/cm-1
Electrical field (kV/cm)
(b)
BSPT/LNO
BSPT/Pt
Pr n / Pr 0 (%)
Switching cycles (log[n])

Figure 7

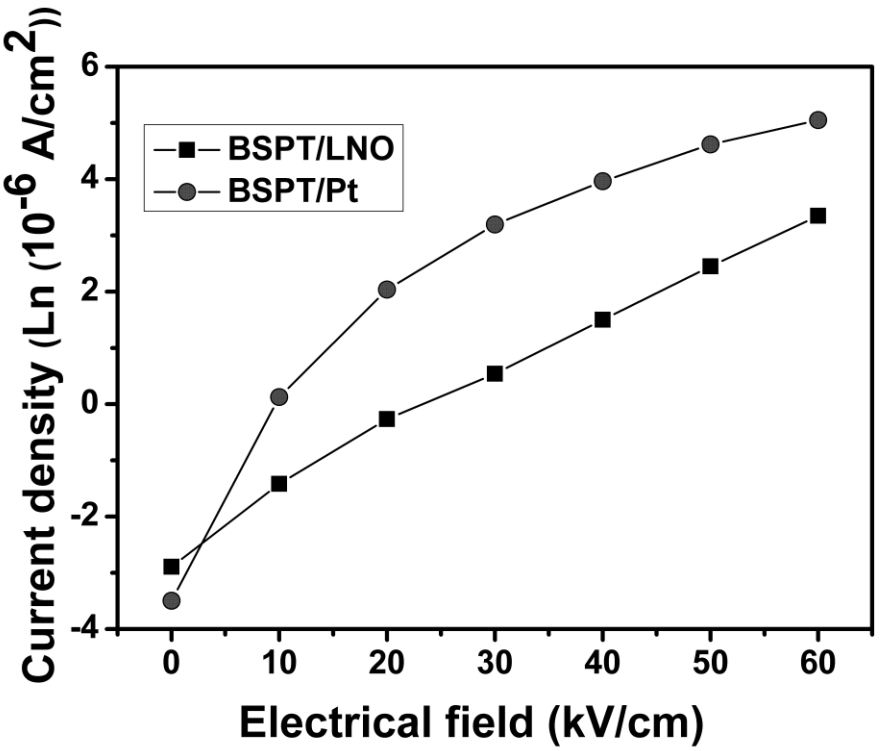
Current density (Ln (10-6 A/cm2))
Electrical field (kV/cm)
BSPT/LNO
BSPT/Pt
6
4
2
0
-2
-4
0
10
20
30
40
50
60

Figure 8

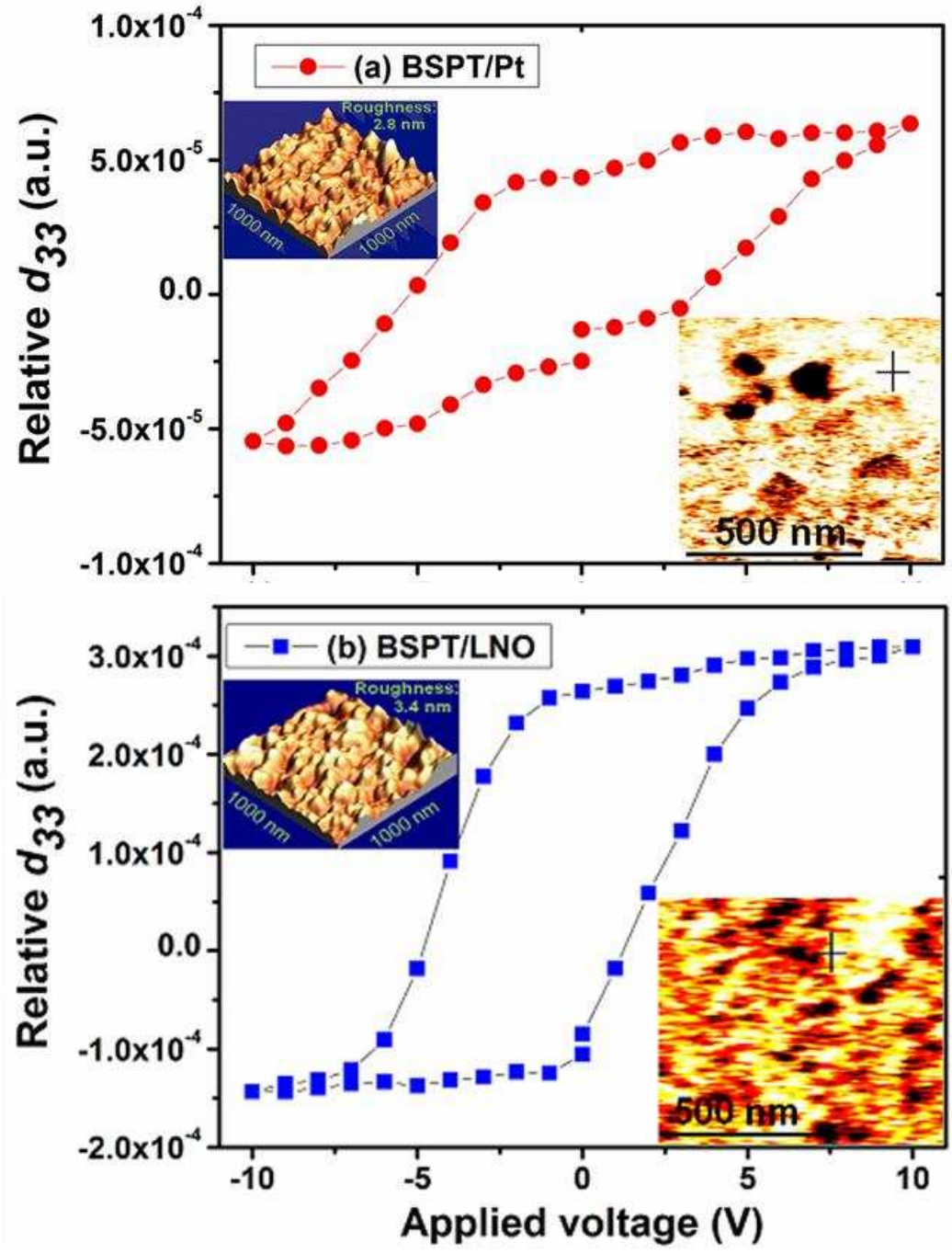
(a) BSPT/Pt
Roughness: 2.8 nm
1000 nm
1000 nm
500 nm
Relative d_{33} (a.u.)
1.0x10^{-4}
5.0x10^{-5}
0.0
-5.0x10^{-5}
-1.0x10^{-4}
(b) BSPT/LNO
Roughness: 3.4 nm
1000 nm
1000 nm
500 nm
3.0x10^{-4}
2.0x10^{-4}
1.0x10^{-4}
0.0
-1.0x10^{-4}
-2.0x10^{-4}
-10
-5
0
5
10
Applied voltage (V)

Figure 9

Table I

Function	Interlayer examples	Ferroelectric film examples	Impact on the ferroelectric films
Seed layer	$PbTiO_3$	PZT[8] BSPT [29]	Facilitate the earlystep for crystallization and formation of perovskite materials
oxide electrode layer	IrO_2	PZT [13] BSPT [30]	Improve the leakage, retention, aging, and fatigue properties in ferroelectrics
buffer layer	BST buffer layer	$BaSrTiO_3$ (BST) [16]	Improve the electrical properties, tailoring the residual stress in the film.
oriented template layer	(La,Sr)Co O3	PZT[17]	Provide a suitable epitaxial template for growth of the overlying perovskite ferroelectric.

Table 2

Lattice and thermal expansion coefficients of the materials, and remanent polazirzaiton of BSPT films on different substrates that related the stress.

Materials	Lattice constant (nm)	Thermal expansion coefficience (K^{-1})	Remanent polarization ($\mu C.cm^{-2}$)
BSPT	0.405	10×10^{-6}	
Pt	0.392	27×10^{-6}	25
LNO	0.384	8.2×10^{-6}	40

For Table of Contents Use Only

Tailoring ferroelectric properties of 0.37BiScO$_3$-0.63PbTiO$_3$ thin films using a multifunctional LaNiO$_3$ interlayer

Jingzhong XIAO[‡†]

Monika TOMCZYK[‡]

Ian M. REANEY[§]

Paula M. VILARINHO[‡*]

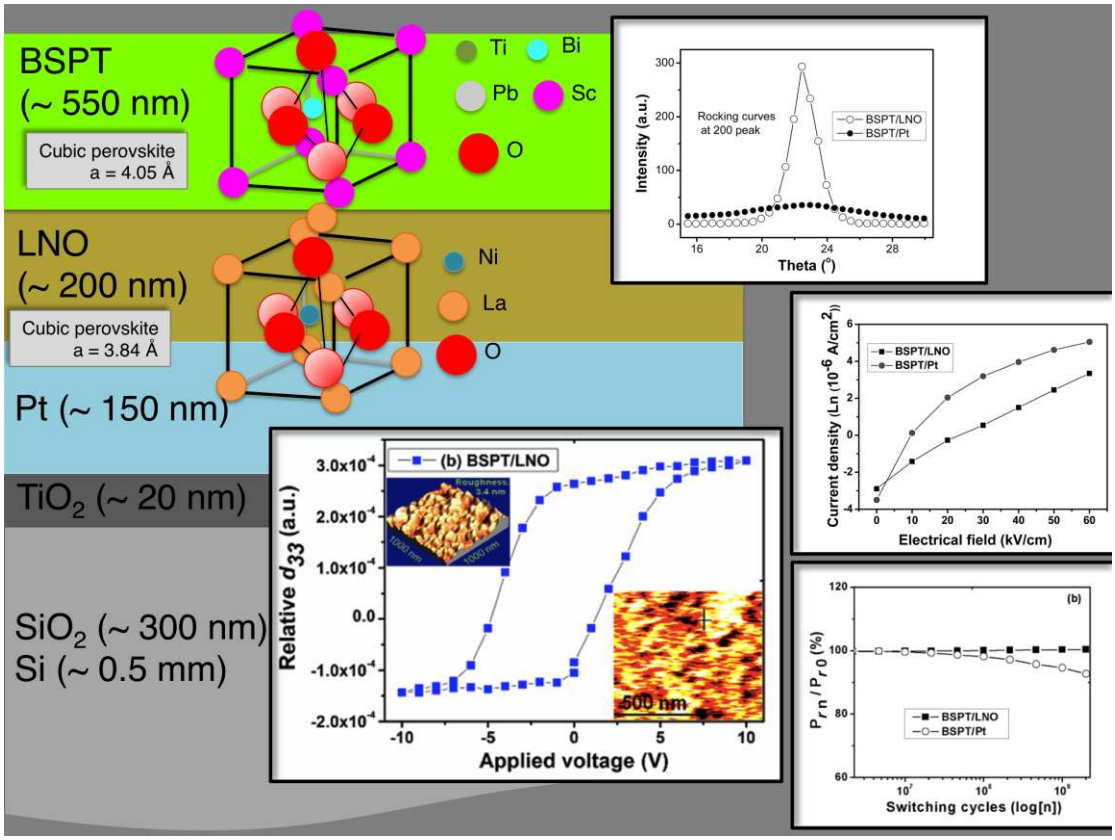

A sol-gel LaNiO$_3$ interlayer on Pt/TiO$_2$/SiO$_2$/Si substrates prior to the growth of sol-gel BiScO$_3$-PbTiO$_3$ films: i) seeds nucleation of the perovskite structure; ii) templates growth, controlled orientation and enhanced crystallinity and iii) acts as a sink for oxygen vacancies. LaNiO$_3$ interlayer not only improves ferroelectric, piezoelectric and dielectric properties but also reduces leakage current and prevents degradation of remanent polarization during fatigue. We propose the use of a LaNiO$_3$ interfacial layer as a generic solution to the interfacial degradation in functional oxide films.